RESEARCH ARTICLE

Path Planning and Trajectory Optimization Based on Improved APF and Multi-Target

JIE YANG[1,2,3]**, HONGCHANG ZHANG**[1,2,3]**, AND PENG NING**[1,2,3]

[1]Hubei Key Laboratory of Advanced Technology for Automotive Components, Wuhan University of Technology, Wuhan 430070, China
[2]Hubei Collaborative Innovation Center for Automotive Components Technology, Wuhan 430070, China
[3]School of Automotive Engineering, Wuhan University of Technology, Wuhan 430070, China

Corresponding author: Hongchang Zhang (zhanghc@whut.edu.cn)

ABSTRACT Aiming at the shortcomings of the path generated by the artificial potential field (APF) method, such as local minimum, target unreachability, and low path smoothness, an improved artificial potential field method is proposed. First, to reduce the collision risk and planning difficulty, based on known environmental information such as the location of obstacles and targets, the area with fewer obstacles is selected as the priority area for path planning. Second, to improve the path smoothness and reduce the computation amount, an adaptive step-size adjustment method based on the distance and angle relationship with obstacles within the prediction range is proposed. Third, in view of the effect on each other between obstacle, local minimum, and unsmooth path, a multi-target model considering the size and influence range of obstacles and an improved potential field function are proposed on the basis of the identified planning priority area. Finally, in order that the path is smooth enough to be tracked by autonomous mobile robots, a safe driving corridor without collision with obstacles is constructed on the planned path, and a trajectory fully constrained to the safe driving corridor is generated using the quadratic programming method. The simulation comparison experiments are carried out on matlab simulation software and the smoothness of IAPF is improved by an average of 97.3% as compared to traditional APF and 45.19% as compared to DWA. The sum of the proposed IAPF path planning and optimization time is improved by 45.1% on average compared to DWA path planning time.

INDEX TERMS Improved APF, multi-target, trajectory optimization.

I. INTRODUCTION

With the development of intelligent technology, autonomous mobile robots (AMRs) have penetrated many industries and are having a significant impact on our lives. For example, unmanned vehicles in factories take over dangerous and repetitive handling tasks for humans. Although AMR can currently complete work according to pre-planned routes in some set scenarios, its development is greatly challenged as the complexity and diversity of tasks and environments increase. Among them, improper path planning may cause the AMR to travel too long and even fail to reach the target, and the complexity of algorithm will also prolong the calculation cycle. In addition, if the size and shape of the AMR and the obstacle are neglected during path planning, the AMR

The associate editor coordinating the review of this manuscript and approving it for publication was Yangmin Li.

may not be able to adjust its direction in some narrow environments, which increases the risk of collision with the obstacle. Therefore, path planning, as one of the main technologies of AMR, has received great attention from both academia and industry.

The purpose of path planning is to plan a collision-free safe path based on known information, which is mainly divided into global and local path planning. There are different requirements for the planned path, according to different usage scenarios and applications. Global path planning includes Dijkstra, A*, ant colony, genetic algorithm, rapid-exploration random tree (RRT) algorithm and reinforcement learning, etc. It is a path planning in a static global environment that has been known, and has poor adaptability to unknown environments. Local path planning includes dynamic window algorithm, artificial potential field (APF) method, etc., which is suitable for path planning in real-time

environments where the environment is unknown or partially unknown. As a popular path planning algorithm proposed by Khatib [1] in 1985, APF has many advantages, such as a mathematical model that is simple and easy to implement, good adaptability to unknown or dynamic environments and so on. It is widely used in active and real-time avoidance of collision [2], [3] and path planning [4], [5], [6] of AMRs.

However, the traditional APF also has the following major disadvantages: (1) the path generated by the APF algorithm may not be smooth or even oscillating; (2) when the resultant force of the potential field forces is zero, the local minimum occurs; (3) when there are obstacles near the target, target unreachability occurs [7]. As path planning has developed, many efforts have been devoted to solving these problems. Some combined APF with other technologies, while others improved the traditional APF [8], [9], [10], [11], [12]. Souza et al. introduced a three-dimensional vortex field into the traditional APF, allowing the robot to automatically and independently select the optimal direction of vortex field rotation based on its position relative to each object in the workspace, eliminating the local minimum problem and oscillations in the influence threshold of the repulsive fields [13]. Li proposed an improved APF that optimized the angle of repulsive force and the function of attraction field, which enabled the robot to avoid local minimum [14]. Shang et al. combined improved APF with fuzzy logic that when the AMR falls into the local minimum, set one or more virtual targets to guide the robot out of the dead zone, which mitigated the occurrence of local minimum and oscillation in the trajectory [15]. Ji et al. converted Cartesian coordinates to ellipsoidal coordinates and converted traditional APF into ellipsoidal two-dimensional APF by solving the Laplace equation. They then integrated the ellipsoidal potential field with the Gaussian velocity field (GVF) to propose a three-dimensional potential field (TriPField) model that simultaneously represents position and velocity. This method solved the shortcomings in the integration algorithm of PF potential field and AV local path planning, such as the neglect of the geometry of the traffic agent and the possible local minimum problem [16]. Szczepanski proposed a safe APF method that the repulsive potential field was replaced by a vortex potential field or a superimposed potential field of the two according to the environment, which could avoid relatively simple situations of local minimum, keep a safe distance from obstacles and pass through narrow corridors [17]. Li et al. proposed an APF method using dynamic enhanced fireworks algorithm (dynEFWA), which used the random explosion of dynEFWA to jump out of local minimum traps and found feasible paths in safe driving areas [18]. In order to consider the influence of positioning accuracy on navigation ability and collision avoidance in path planning, Shin and Kim proposed to mix potential energy and position risk field to generate a hybrid directional flow to guide an UV in a safe and efficient path [19]. Sfeir et al. redefined a form of repulsion potential field based on APF method to reduce trajectory oscillations when the

robot approached obstacles [20]. Zheng et al. proposed a new minimum criterion and designed an improved virtual obstacle method for local path planning to overcome the drawback [21]. Matoui et al. used the non-minimum speed algorithm to solve the local minimum problem [22]. Duan et al. added the interference factor of the second virtual target in the improved APF based on the safe distance model (SDM), so as to break the equilibrium state when falling into a local minimum [23]. Szczepanski proposed a novel APF supported by augmented reality that could extend robot perception, detect upcoming local minimum, and generate a virtual wall to bypass it, which relatively reduced the driving path, but failed to consider the smoothness of the path [24]. Yao et al. proposed a method named black-hole potential field(BHPF) to reduce the occurrence of local minimum, then combined BHPF and reinforcement learning to solve the problems which are scenarios of local-stable-points. This adaptation mechanism enabled the robot to reach the destination in real time in environments with novel obstacles and dynamic targets, but the size of the black hole domain must be defined for different environments. Moreover, the algorithm was not adaptable enough, and the smoothness of movement was not improved [25]. Szczepanski proposed a novel APF improved by application of the prediction of future movements, to detect AMR's stagnation in the local minimum. In such a case, the virtual obstacles, called top quarks, were created to force the AMR to select goal-reaching path. However, when placing a virtual top quark, the procedure of prediction of future path was repeated until the local minimum point no longer appears, which undoubtedly greatly increased the amount of calculation, but also led to poor real-time performance [26]. Azzabi et al. proposed a novel of repulsive potential function by activating a virtual escaping force when a local minimum was detected. This force behaved as a rotational force allowing the robot to escape from the deadlock positions and turn smoothly away from obstacles in the direction of the target. And a stronger attractive function was proposed to ensure that the robot reaches the target successfully. The combination of the new attractive force and the novel repulsive force could solve the local minimum and the unreachable target problem [27]. Guo et al. proposed an adaptive step size adjustment method based on the number of obstacles, the distance between the robot and the obstacles, and the number of iterations to improve the efficiency of path planning and obstacle avoidance; proposed triangulation navigation method to get out of the stagnant situation when falling into the local minimum; improved the potential field function so that the closer the robot was to the target, the smaller its repulsive component and the greater the attractive component, thereby solving the problem of target unreachability [28]. Li et al. introduced the invasive weed method to help solve the local minimum problem and added a distance adjustment factor on the basis of the original repulsive potential field to solve the unreachable target problem [29]. Zhai et al. proposed to improve the potential field environment and

potential field force to solve the two problems, but the method was less adaptable in a complex environment with multiple obstacles [30]. Song et al. added a predicted potential field to the original APF that If it predicted the risk of collision, the direction of movement would be corrected to avoid the obstacle in advance. However, the algorithm was only applicable to single-obstacle environment, for in multi-obstacle environment the modified direction might collide with other obstacles. Moreover, it did not contain local minimum avoidance mechanism [31]. Batista et al. proposed a virtual obstacle model and modified the repulsion function to solve the unreachable target problem. However, the algorithm used the equal-step path method and the overall planning efficiency was not high [32].

The most well-known and concerned problem in most of the above studies is the case of falling into local minimum, but no study addresses all of the three main flaws of APF in the meantime and considers their effect on each other. The above studies have the following problems: (1) Most do not consider the size of obstacles, but only regard obstacles and the robot as a particle, which is inconsistent with the actual situation. In this paper, square obstacles of different sizes will be introduced for study, because sharp corners and boundaries of squares make it more difficult to do path planning than circles. (2) Most only solve the problem of local minimum or target unreachability, but ignore the influence of unsmooth path on the entire motion process. (3) Most only propose separate solutions for individual problems, without considering multiple problems together while reducing the complexity of the algorithm. (4) There are two main mechanisms for avoiding local minimum. One begins to work after the robot has fallen into the local minimum, so that the smoothness of the path cannot be guaranteed; Another is to repeatedly detect all locations where local minimum may occur throughout the whole planning process, and then add virtual obstacles or modify potential field functions, which greatly increases the amount of calculation.

Therefore, this paper considers the three problems of traditional APF together, and proposes an improved APF algorithm to solve the problems of local minimum and target unreachability when obtain relatively short and smooth trajectories. The structure of this paper is as follows: Section II describes the traditional APF algorithm, especially the drawbacks; Section III presents the proposed approach, including the selection of the planning area and the construction of multi-target planning based on environmental information, the improvement of repulsive force field and attraction function, the adaptive adjustment of step size according to the distance and angle relationship with obstacles within a certain prediction range, the construction of safe driving corridors based on path points generated by multi-target, and the generation of smooth trajectories using safe driving corridors as boundary constraints. Section IV presents and analyzes the simulation results solving the three problems. Section V summarizes the paper and discusses future work.

II. TRADITIONAL ARTIFICIAL POTENTIAL FIELD ALGORITHM

The well-known APF proposed by Khatib in 1986 has developed over decades with different modifications. It is widely used in path planning, consisting of repulsive potential field and attractive potential field, which are similar in principle to the positive and negative electric fields respectively. The repulsive potential field is like a positive electric field, whose potential field force is dispersed from the center to the outside and is repulsive to the AMR, while the attractive potential field is like a negative electric field, whose potential field force is converged from the outside to the center and is attractive to the AMR. The two work together to guide the AMR away from the obstacle and toward the target.
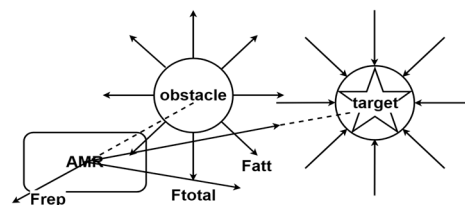

FIGURE 1. Force diagram of AMR in APF.

The AMR is subject to both attractive and repulsive forces in the APF with target and obstacle. The attractive force guides the AMR to travel toward the target point, while the obstacle exerts repulsive force after the AMR enters the influence range of its repulsive field, which makes the AMR move away from it to avoid collision, as shown in Fig. 1.

When an AMR is in an APF containing a target, it will be attracted by the target until the AMR reaches it. The attractive potential field function of the traditional APF is:

$$U_{att} = \frac{1}{2}k_{att}\left(P - P_{target}\right) \tag{1}$$

where k_{att} is the attractive coefficient, P is the position of the AMR, P_{target} is the position of the target.

The negative gradient of the attractive potential field is the gravity:

$$F_{att} = -grad(U_{att)} = k_{att}\left(P_{target} - P\right) \tag{2}$$

The repulsive potential field function of an obstacle is:

$$U_{rep} = \begin{cases} \frac{1}{2}k_{rep}\left(\frac{1}{P} - \frac{1}{R_0}\right)^2, & 0 \leq P \leq R_0 \\ 0, & R_0 \leq P \end{cases} \tag{3}$$

where, k_{rep} is the repulsive factor, P is the distance between the AMR and the obstacle, and R_0 is the maximum influence range of the repulsive potential field belonging to the obstacle. When there is an obstacle in the APF and the AMR is under the influence range of the obstacle's repulsive field, the AMR will be subjected to the repulsive force. After leaving the influence area, it will not be affected by the obstacle.

The negative gradient of the repulsive potential field is:

$$Frep = \begin{cases} k_{rep} \left(\dfrac{1}{P} - \dfrac{1}{R_0} \right) \dfrac{\vec{P}}{P^2}, & 0 \le P \le R_0 \\ 0, & R_0 \le P \end{cases} \quad (4)$$

So, the final resultant force on the AMR in the APF is:

$$Ftotal = \sum Frep + Fatt \quad (5)$$

where $\sum Frep$ denotes the total repulsive force that the AMR is subjected to when under the influence of multiple obstacle repulsive fields, and the attractive and repulsive forces are superimposed to form the resultant force that the AMR is subjected to in the APF.
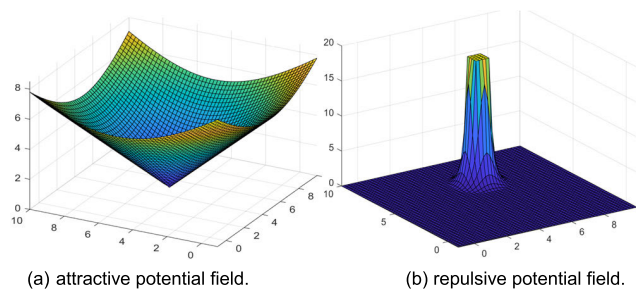

(a) attractive potential field. (b) repulsive potential field.

FIGURE 2. Traditional artificial potential field diagram.

From the traditional APF repulsive force function, it can be seen that its derivative is not 0 at the boundary of the obstacle's repulsive field influence area, because the repulsive field is not tangent to the 0-potential energy surface. At the same time, it can be seen from (b) that the gradient of the obstacle's repulsive field decreases very fast, which can bring some problems. If the step of the traditional APF is not properly selected, it is easy for the situation that in the previous step the AMR is outside the repulsive field of an obstacle, but in the next step it is deep inside the repulsive field, which will make the AMR be subject to a suddenly increasing repulsive force, so as to be directly ejected from the repulsive field. Such a sudden change in the path point is very inconsistent with the actual situation.

III. IMPROVED APF AND TRAJECTORY GENERATION

For the collision-free path planning problem, firstly, analyze the known map information to restrict the path planning to the area with fewer obstacles, and then evaluate the obstacles that must be avoided when traveling from the starting point to the target point. Secondly, construct a multi-target model by setting up sub-target points within a certain range near the obstacles in which the resultant force of the target ahead and the next target can guide the AMR away from the obstacles. In this way, the AMR will travel toward the point that must be passed by avoiding the obstacles and the next target with a variable stride length, until it reaches the final target. Thirdly, the safe driving corridor is constructed according to the path points generated by the front-end processing. Finally, the safe driving corridor is used as a boundary constraint to generate

a smooth trajectory that is contained in the safe driving corridor.

The algorithm effectively avoids local minimum, while planning relatively short and smooth paths, and also provides a large improvement in target unreachability case.

Planning path in unstructured scenarios is more challenging compared to highway cruising because 1) there is no longer a navigational reference line, 2) the planned path usually contains cusps instead of smooth curves, and 3) obstacles are more irregular than those on structured roads. Due to these factors, very little research has been done to generate smooth trajectories in unstructured scenarios considering obstacle size. This study focuses on the generation of collision-free smooth trajectory in complex scenarios with irregularly placed static obstacles.

A. PRIORITY AREA SELECTION AND MULTIPLE TARGETS CREATION

1) PSFO-BASED PRIORITY AREA SELECTION

Since the risk of collision and the difficulty of path planning are directly proportional to the number of obstacles, the selection of an appropriate area is extremely important for planning a safe collision-free smooth path. In this paper, a priority area strategy for path planning based on the principle of side with fewer obstacles (PSFO) is proposed, which can determine the path planning area based on the positional relationship between the robot, obstacles, and targets. First, before the path planning starts, connect the starting position of the robot and the final target with a straight line, and the number of obstacles on each side of this line is analyzed and calculated. Then the side with less obstacles is selected as the path planning priority area.

2) MULTIPLE TARGETS CREATION

In the traditional APF method, the robot moves in the whole potential field according to the resultant force of the attractive force of the final target and the repulsive force of obstacles. Since the final target is a single-point model and its attractive force is related to the distance: the larger the distance is, the larger its attractive force is; the smaller the distance is, the smaller its attractive force is. When the robot is far away from the final target, its attractive force is very large, and it may appear that the attractive force on the robot is much larger than the repulsive force of the obstacle on the robot in some positions, which greatly increases the risk of collision in traveling. Besides, it makes the robot avoid collision only when it enters into the influence range of the repulsive field of the obstacle, which greatly increases the traveling distance and reduces the smoothness of the path.

If directly plan a point that the robot must pass through to avoid the obstacle, we can solve the problem of unsmooth path, greatly reduce the risk of collision, shorten the driving distance, and also avoid possible local minimum. Sang et al. proposed an improved APF algorithm, which generates a globally optimal path by improving the A* algorithm and

divides the optimal path into a sequence of sub-target points [33]. Although it can reduce the probability of falling into local minimum, it increases the algorithm complexity and computation amount. This paper proposes a lateral safety target generation method based on the radius of the influence range of obstacles' repulsive field to create multiple targets, which can consider collision avoidance, path smoothness and local minimum avoidance simultaneously without increasing the algorithm complexity. The specific approach is as follows:

1) Based on the line connecting the start point to the final target, the distance of all obstacles to this line is calculated;

2) If the distance from a certain obstacle to the link is less than its repulsive field influence range, the obstacle should be avoided during the actual traveling of the robot. As for the lateral safe distance for the robot to avoid the obstacle, it is related to the repulsive field influence range of the obstacle. To select the lateral safety target point, a straight line perpendicular to the line connecting the starting point to the final target should be made through the center coordinates of the obstacle. And along this straight line in the direction of the selected path planning area, a point where the distance to the line is equal to the lateral safety distance should be found, which will be used as a lateral safe sub-target of the path. The lateral safe distance is selected as $d_{safe} = k_1 R_0$, where k_1 is a certain scale factor and R_0 is the influence range of the repulsive field corresponding to a certain obstacle. The lateral safe distance should be chosen so that the AMR is far away from the obstacle, but not completely out of the influence of its repulsive field.

The lateral safe target strategy can effectively solve two typical local minimum cases. The first one is when the obstacle is at a point on the line between the AMR and the final target, the traditional APF method will lead to the resultant force of attractive and repulsive forces on the robot zero, producing a local minimum. Shahidian and Soltanizadeh defined an additional collision avoidance condition and introduced an improved algorithm to avoid this case [34]. The second case is when there are two or more obstacles between the AMR and the final target, and they are distributed near the line connecting the AMR and the final target. In this case, the produced repulsive forces can offset the attractive force of the target point, so that the resultant force on the AMR is zero and falls into a local minimum.

For the first case, the obstacle is located on the line connecting the AMR and the final target, and must be avoided by the AMR in the multi-target strategy, as shown in Fig. 3(a).

The second case is a little bit more complicated because the obstacles are distributed on both sides of the line. Firstly, if the distance of two obstacles on both sides of the line is larger than the AMR size, the local minimum will definitely appear between the two obstacles. Based on that, sub-target points between the two obstacles will be generated to guide the AMR to pass through these obstacles without collision,
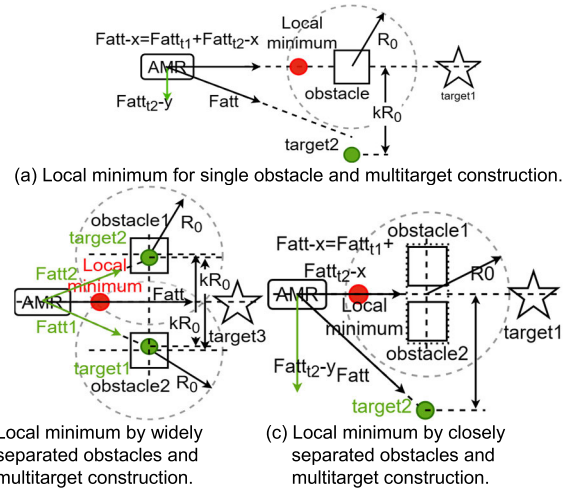

(a) Local minimum for single obstacle and multitarget construction.

(b) Local minimum by widely separated obstacles and multitarget construction.

(c) Local minimum by closely separated obstacles and multitarget construction.

FIGURE 3. Typical local minimum cases and multi-target point setting.

as shown in Fig. 3(b). Secondly, if the distance of the two obstacles on both sides of the line is smaller than the AMR size, the repulsive potential fields of these obstacles will overlap with each other. In this case, these obstacles will be regarded as a large obstacle to be avoided. Similar to the first case, multiple targets are generated in the priority planning area to guide the AMR to avoid them collision-free, as shown in Fig. 3(c).

B. IMPROVEMENT OF THE POTENTIAL FIELD FUNCTION

1) IMPROVEMENT OF THE ATTRACTION FUNCTION FOR THE CONSTRUCTION OF A MULTI-TARGET ATTRACTION FIELD

Due to the drawbacks of single-point attractive field (as described in III-A2)), we adopt a multi-target model based on multiple sub-target points where the attractive potential fields of two adjacent sub-target points in front of the AMR are superimposed in a certain proportion through hyperbolic tangent function. It aims to consider the attractive force of the second sub-target point when the AMR travels toward the first sub-target point, which is conducive to further reducing the possibility of falling into the local minimum; And lift the guidance of the first sub-target point when the AMR is about to arrive at the first sub-target point ahead. But the guidance will be continued by the second and third sub-target points ahead, and so on. The equation is as follows:

$$y = tanhx \qquad (6)$$

$$k_2 = \frac{d_{rob-subtar(i)}}{d_{rob-subtar(i+1)}} \qquad (7)$$

$$Fatt = Fatt_{(i)} + tanh(k_2) Fatt_{(i+1)} \qquad (8)$$

where $d_{rob-subtar(i)}$ is the distance from the AMR to the ith sub-target point ahead, $d_{rob-subtar(i+1)}$ is the distance from the AMR to the $i + 1^{th}$ sub-target point ahead, and accordingly k_2 is the ratio of the distance from the AMR to the ith sub-target point ahead to the distance from the AMR to the $i + 1^{th}$ sub-target point ahead. $Fatt_{(i)}$ and $Fatt_{(i+1)}$ are the attractive force of the ith and $i + 1^{th}$ sub-target to the AMR, respectively.

When the AMR reaches the front of the last sub-target point, the guidance of the final target point to the AMR can be increased, so the attractive function at this stage is as follows:

$$Fatt = k_3 Fatt_{ft} + Fatt_{ilast} \qquad (9)$$

where k_3 is the is a coefficient($0 < k_3 < 1$), $Fatt_{tt}$ and $Fatt_{ilast}$ are the attractive force of the final target and last sub-target to the AMR, respectively.

After passing the last sub-target point, the attractive force on the AMR is supplied only by the final target point:

$$Fatt = Fatt_{ft} \qquad (10)$$

2) IMPROVEMENT OF THE REPULSIVE FORCE FIELD

According to the repulsive force potential field diagram made by the repulsive force function of the traditional APF method, it can be seen that the smaller the radius of the obstacle, the larger the repulsive force field at its boundary. It is contrary to the rule in the real environment that the larger the obstacle, the higher the risk of collision, and the larger the needed repulsive force. Moreover, the gradient of the repulsive force field of a conventional APF decreases extremely fast, as shown in Fig. 4(a). This can lead to the appearance of a point near the obstacle that is subjected to an extremely large repulsive force, making the generated path have mutation points, as shown in Fig. 6(a).
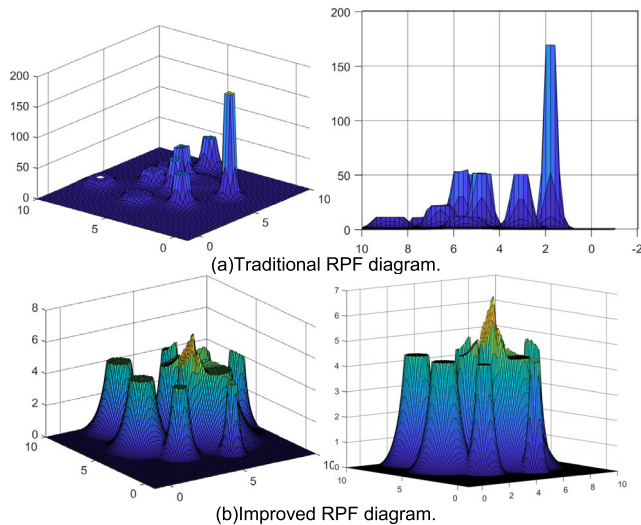

(a)Traditional RPF diagram.

(b)Improved RPF diagram.

FIGURE 4. Repulsive potential field before and after improvement.

Therefore, it is necessary to improve the repulsive force function so that the gradient of the repulsive potential field will not fall so fast, and that the tangent of the repulsive potential field contour is also 0 when the height is 0, in order to ensure that the repulsive potential field is in smooth transition with the zero repulsive potential surface. Inspired by the hypoellipse curve (Lamé curve), when the exponent parameter of this curve is less than 1, the shape of the curve resembles an inwardly concave four-pointed star, and the curve is tangent to the coordinate axes, as shown in Fig. 5. It is more in line with the rule that outside the influence range

of the field the repulsive force is 0, but within the range the repulsive force gradually increases as closer to the obstacle, and an upper limit is set for the force so that it will not increase to infinity.
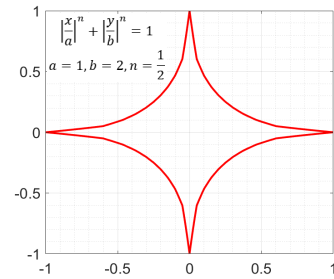

FIGURE 5. Lamé curves with parameters that satisfy the condition that the curve is tangent to the coordinate axes.

Based on the above analysis, the curve $\left(\frac{x}{rho\_0}\right)^{0.5} + \left(\frac{y}{Fre_{max}}\right)^{0.5} = 1$ is taken to improve the repulsive force function, and the improved function is:

$$Fre = Fre_{max}\left(1 + \frac{rho - r}{rho\_0} - 2\sqrt{\frac{rho - r}{rho\_0}}\right) \qquad (11)$$

where rho is the distance of the AMR from the obstacle, r is the distance from the center of the obstacle to its boundary, rho_0 is the radius of influence range of the repulsive field of the obstacle, and Fre_{max} is the repulsive force on the boundary of the obstacle, which is the same order of magnitude as the maximum attractive force $Fatt_{max}$. The improved potential field diagram of the repulsive field is shown in Fig. 4(b).

After improving the repulsive force function, the situation of mutation points by the sudden larger repulsive force near the obstacle no longer appears, and the path is smoother compared to the original one, as shown in Fig. 6.

C. PREDICTION-BASED ADAPTIVE STEP

In this paper, the step is adaptively adjusted according to the distance and angle relationship of the AMR with obstacles within a certain prediction range. In the traditional APF method, the step length is always kept constant during the robot's traveling, which is not in line with the actual situation of decelerating when encountering obstacles and accelerating when there are no obstacles. Meanwhile, If the step size is kept small, it is easy to cause excessive calculation and too-curved path; if the step length is kept large, it is easy to collide with obstacles in some complicated situations. Therefore, in order to improve the smoothness of the planned path and increase the safety in traveling, the length of each step in the robot's traveling process is set to be variable. Before each step of movement, the robot's current force situation and future movement direction will be evaluated to see whether there is an obstacle within a certain distance and a certain angle ahead. If no obstacle is detected ahead, the path ahead can be considered as hazard-free and the robot can advance with maximum step length; if an obstacle is detected in front,

the robot will automatically adjust the forward step length according to the distance from the obstacle. The further the distance, the smaller the risk of collision, and the forward step length can be appropriately increased; the closer the distance, the greater the risk of collision, and the forward step length should be reduced, as shown in Fig. 6.

At the same time, since the AMR in this paper adopts the step length adaptive adjustment, the combination of the forward detection results and the forward step length adjustment can solve the target unreachability problem in the APF algorithm when there is an obstacle near the final target point. In the traditional APF method, when there is an obstacle near the final target, as the robot gets closer to the target, the attractive force on the robot will become smaller while the repulsive force will become larger, thus the repulsive force is larger than the attractive force on the robot at a certain position, which makes the robot unable to reach the final target. However, through the adaptive adjustment of the step length, when the robot is close to the final target, the distance between the target and the robot within the prediction range can be used to adjust the step length of the robot, that is, the next step length is calculated according to a certain proportion of this distance. This is also in line with the actual situation that when the robot is approaching the target point, it will gradually decelerate to reach the final target smoothly.
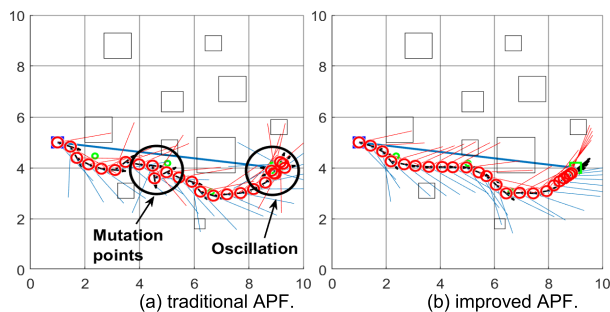

FIGURE 6. Path planning based on the adaptive step strategy.

D. CONSTRUCTION OF SAFE DRIVING CORRIDORS BASED ON PATH POINTS GENERATED BY MULTI-TARGET MODEL

After obtaining n APF path points generated by multi-target model, it is found that the improved APF is much smoother than the path generated by traditional APF, but there is still much room for optimization. Moreover, it is also found that the path generated by the APF method has a great dependence on environmental factors such as obstacles and target points. At some points, problems such as turns with unsuitably large angle may occur, which can hinder the AMR tracking. So, further smoothing of the path is necessary. However, how to ensure that the smoothed trajectory does not conflict with surrounding obstacles is an issue worth pondering. The paper draws on the fight corridor in AMR online safe trajectory generation [35], [36], [37] and applies the idea to 2D map for generating safe driving corridors without collision with obstacles. In this way, the safe driving corridor is used as the

boundary constraint, which ensures that a safe and collision-free optimized trajectory can be generated.

In this paper, the collision-free space around the path is extracted to form a safe driving corridor for subsequent path optimization. Here is the concrete process: From the starting point, connect the first point and the third point (point i and point i+2). Then, translate this line segment to the left and right to determine the boundaries on the left and right sides of the safe driving corridor, with a maximum offset of D. In the process of constructing the corridor, detect whether the generated corridor intersects with any obstacle in each movement. If the line segment does not intersect with any obstacle, the line with an offset of D will be taken as the boundary line of the corridor on that side; if the line segment intersects with an obstacle, then the offset is reduced by one unit and the line segment returns to the position of the previous step where it has not intersected with the obstacle. The returned line is used as the corridor boundary line on that side. The process is repeated until the construction of a corridor between the $n - 2^{th}$ point and the nth point. The corridors generated by each corresponding line segment are assembled as the boundary constraints for the next step of trajectory optimization, as shown in Fig. 7.
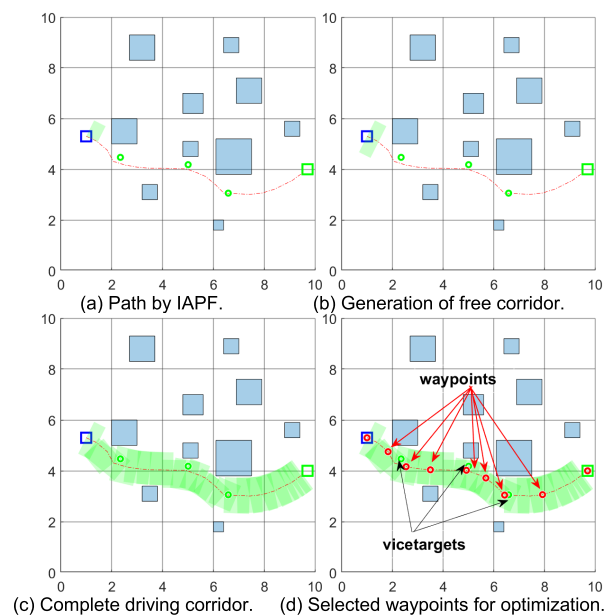

FIGURE 7. Construction of safe driving corridors. The path planned by the improved APF is shown as the red curve. And the corridors is shown as the green shadow.

After generating the safe driving corridor, it is noted that trajectory optimization in this area is particularly necessary to ensure that the generated trajectories do not exceed the boundary of turns that are generated by the APF repulsive force. In order to save computation cost and running time, the number of sequences and waypoints can be set to the number of sub-target points, but at the same time, to ensure that the generated trajectory points are all within the safe driving corridor, the midpoints of the adjacent target points are taken

and inserted into the waypoint sequence. The path generated by the APF does not completely pass through the sub-targets selected during the planning, but deviates to a certain extent according to the actual situation, as shown in the figure above. Therefore, in order to carry out the next step of trajectory optimization, it is necessary to re-select the waypoints. In this paper, the closest points to the location of the waypoints on the generated APF path are chosen as the reference waypoints in the final optimization process, as shown in Fig. 7(d).

E. PATH OPTIMIZATION WITH SAFE DRIVING CORRIDOR CONSTRAINTS

In this section, a quadratic programming approach is applied to generate trajectories constrained in the safe driving corridor. The trajectory consisting of segmented polynomials is parameterized as the time variable t in x, y.

1) POLYNOMIAL TRAJECTORY GENERATION

The optimized trajectory is represented by a k-segment n-order segmented polynomial, given the start and end time of each segment $(t_0, t_1, t_2, \ldots, t_k)$. Since the trajectory in real problems is two or three dimensional, each of which is usually solved separately. Both the horizontal and vertical coordinates can be represented by the following equation:

$$p(t) = \begin{cases} [1, t, t^2, \ldots, t^n] \cdot p_1 \ t_0 \leq t < t_1 \\ [1, t, t^2, \ldots, t^n] \cdot p_2 \ t_1 \leq t < t_2 \\ \ldots \\ [1, t, t^2, \ldots, t^n] \cdot p_k \ t_{k-1} \leq t < t_k \end{cases} \quad (12)$$

$$p_i = [p_{i0}, p_{i1}, \ldots, p_{in}]^T \quad (13)$$

where k is the number of segments of the trajectory, p_{ij} is the coefficient of the i-segment, j-order polynomial, and p_i is the parameter vector of the i-segment of the trajectory. We intend to solve for the parameter vectors that satisfy the constraints of the trajectory, and the cost function is the square of the Nth derivative. In this paper, the jerk will be minimized along the trajectory, i.e., N^{th} is taken to be 3, and the objective function can be written as

$$J = min \int_0^T \left(\frac{d^{N^{th}} p(t)}{dt^{N^{th}}} \right)^2 dt \quad (14)$$

The function can be simplified as $min p^T Q p$, where $p = [p_1^T, p_2^T, \ldots, p_k^T]^T$ is the vector of all segment trajectory parameters, Q is the Hessian matrix of the function, and

$$Q = \begin{bmatrix} Q_1 & & & \\ & Q_2 & & \\ & & \ddots & \\ & & & Q_k \end{bmatrix}.$$

2) IMPOSING CONSTRAINTS

Since the trajectories are polynomially spliced, smooth transitions between segments should be ensured, and the planned trajectories should be within safe driving corridors to ensure safety.

a: POSITIONAL CONSTRAINT

Firstly, at the first and last endpoints of the whole trajectory, mandatory constraint is used to fix the start point of the first segment trajectory and the end point of the last segment trajectory at the start and end points of the planning, respectively. As for the constraints of the intermediate connecting points, floating constraints is used to make the adjacent two connecting points have the same position, velocity and acceleration, rather than to fix the position of the adjacent two connecting points at a certain place, which is conducive to the smoothness of the whole trajectory.

b: CONTINUITY CONSTRAINT

The two adjacent end trajectories must be continuous, i.e., the end point of the i-segment trajectory and the start point of the i+1-segment trajectory need satisfy the M-order derivation continuity $(0 \leq M \leq N^{th} - 1) : p_i^{(M)}(t_i) = p_{i+1}^{(M)}(t_i)$.

c: SAFE DRIVING CONSTRAINT

According to the above constraints we have been able to solve the quadratic programming problem, but the generated trajectory only ensures that the curve is continuous and smoothly transitioned, and does not guarantee that the optimized curve does not conflict with obstacles in the map. So, it is necessary to add additional constraints to it to make sure that the generated trajectory must be in the safe driving corridor generated in III-D.

$$\begin{cases} p_i(t_i) - corridor(x_i)_{lower} \leq p_{ix}(t_i) \\ p_i(t_i) + corridor(x_i)_{upper} \geq p_{ix}(t_i) \end{cases}$$
$$\begin{cases} p_i(t_i) - corridor(y_i)_{lower} \leq p_{iy}(t_i) \\ p_i(t_i) + corridor(y_i)_{upper} \geq p_{iy}(t_i) \end{cases} \quad (15)$$

where $corridor(x_i)_{lower}$ and $corridor(x_i)_{upper}$ are respectively the upper and lower limits of the safe driving corridor in dimension x for the trajectory points on i-segment at t_i. Similarly, $corridor(y_i)_{lower}$ and $corridor(y_i)_{upper}$ are respectively the upper and lower limits of the safe driving corridor in dimension y for the trajectory points on i- segment at t_i. And any *corridor* is less than D.

Position constraint, continuity constraint, and safe driving constraint can all be translated into solutions for optimizing the parameter vectors of each trajectory segment $p_i = [p_{i0}, p_{i1}, \ldots, p_{in}]^T$. The position constraint and continuity constraint can be formulated as equation constraint on the objective function, while the safe driving constraint is formulated as inequation constraint on the objective function. It can be seen that the trajectory optimization problem is transformed into a quadratic programming problem:

$$min p^T Q p$$
$$s.t. A_{eq} p = b_{eq}$$
$$A_{ieq} p \leq b_{ieq} \quad (16)$$

Solving this quadratic programming problem yields the optimized smooth trajectory. In section III-D., it is proposed to insert midpoints between adjacent points in the original multi-target sequence to ensure that the generated trajectory is completely within the safe driving corridor. In this section, solutions are presented for both cases. As shown in Fig. 8, the trajectory with more waypoints needs more constraints which reduce the possibility of the trajectory to exceed boundaries of the safe driving corridor. The insertion of intermediate points between the original waypoints as proposed in III.D. is proved to be necessary.
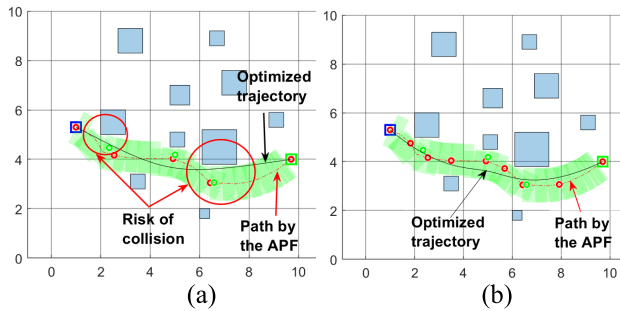

FIGURE 8. (a) Trajectory optimization when the number of waypoints is equal to the number of multiple target points. (b) Trajectory optimization when intermediate points between waypoints are inserted.

IV. SIMULATION AND ANALYSIS

In section I, we pointed out that the traditional APF has the problems of local minimum, target unreachability, and non-smooth paths. In section III, we proposed a multi-target strategy based on the improved potential field function considering environmental factors, and trajectory optimization is performed using the generated path points. In this section, the proposed method is verified in some scenarios.

A. AVOIDANCE OF LOCAL MINIMUM

1) SINGLE OBSTACLE SITUATION

When the obstacle is between the AMR and the target point, and the center coordinates of the three are in a straight line, as the AMR travels toward the target point, at a point on the line of the three will appear the situation that AMR is subject to attraction of the target point and repulsion of the obstacle which are equal in size and opposite in direction. At this time, the resultant force is 0, and the AMR will fall into a stagnant state. The simulation results are shown in Fig. 9(a).

In the improved APF algorithm, after the algorithm analyzes the known map information, multi-target method is applied to generate the sub-target point that must be passed to avoid obstacles and local minimum. And then the multi-target model guides the AMR to avoid them. The improved APF algorithm can successfully avoid local minimum to reach the target point, and the generated path is smoother, as shown in Fig. 9(b). And the comparison of simulation data for TAPF [1] and IAPF is shown in Table 1.
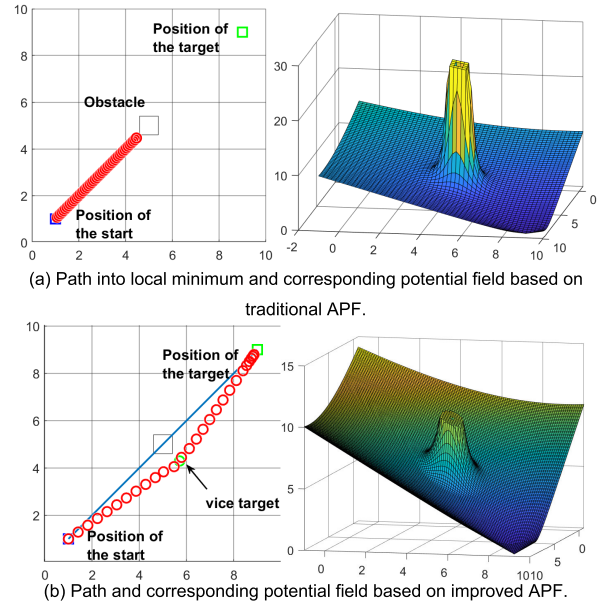

FIGURE 9. Simulation results for single obstacle before and after APF improvement.

TABLE 1. Simulation results of local minimum for single obstacle.

	Start	Obstacle	Target(s)	Iteration
TAPF	(1, 1)	(5, 5)	(9.0, 9.0)	Infinite
IAPF	Ditto	Ditto	(5.85, 4.15) (9.0, 9.0)	28

2) MULTIPLE OBSTACLES SITUATION

When the AMR is in a complex environment of multiple obstacles, it is easy to fall into a local minimum, as shown in Fig. 10(a). In the improved algorithm, the known map information is also analyzed first to select the area with lower collision risk, and then the multi-target method is used to generate the sub-target points that must be passed to avoid obstacles and local minimum. Next, the multi-target model guides the AMR to the target, as shown in Fig. 10(b). The improved APF algorithm does generate multiple targets for obstacle avoidance and local minima, and there is little iteration after successfully reaching the final target, as shown in Table 2.

TABLE 2. Simulation results of local minimum for multi-obstacles.

	Start	Obstacle	Target(s)	Iteration
TAPF	(1, 6)	(3.5, 3.1), (2.5, 5.5) (5.2, 6.6), (6.8, 4.5) (7.4, 7.1), (5.1, 4.8) (3.2, 8.8), (6.7, 5.7) (6.2, 1.8), (9.1, 5.6)	(9.0, 4.8)	Infinite
IAPF	Ditto	Ditto	(2.3, 4.5), (5.0, 4.2) (6.6, 3.1), (9.0, 4.8)	30

B. IMPROVEMENT OF THE TARGET UNREACHABILITY

The first scenario of target unreachability in this paper is that there are several obstacles to be avoided between the AMR departure point and the final target point, and the final target point is behind a larger obstacle and within the
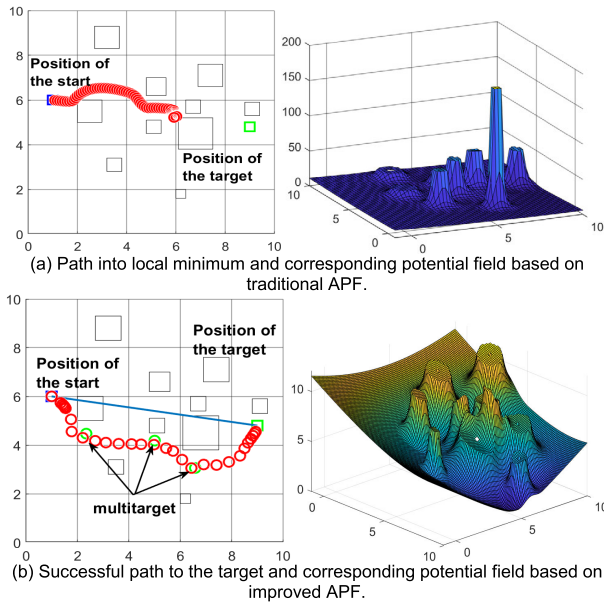
FIGURE 10. Simulation results for multiple obstacles before and after APF improvement.

FIGURE 11. Simulation results for multiple obstacles before and after APF improvement.

repulsive potential field of the obstacle. The path planned by the traditional APF can lead to the situation of target unreachability, and collide with the boundary of the obstacle. But using the improved APF method, the AMR, guided by the multi-target model, continuously detects obstacles and targets in the prediction range in front of it and automatically adjusts its step size and the resultant force size, so that it can successfully reach the final target without collision, as shown in Fig. 11(a).

Another scenario is that the final target point is between two or more obstacle potential fields, and the traditional APF also cannot ensure the reach of target point. But using the improved APF method, the multi-target model can guide the AMR to the target successfully, as shown in Fig. 11(b). The iteration number of the proposed method is small, while that of the traditional APF is infinite in the following two scenarios, as shown in Table 3.

TABLE 3. Comparison of simulation results for target unreachability.

		Start	Obstacle	Target(s)	Iteration
Scenario 1	TAPF	(1, 5)	(3.5, 3.1), (2.5, 5.5) (5.2, 6.6), (6.8, 4.5) (7.4, 7.1), (5.1, 4.8) (3.2, 8.8), (6.7, 8.9) (6.2, 1.8), (9.1, 5.6)	(8.0, 4.7).	Infinite
	IAPF	Ditto	Ditto	(2.4, 4.2), (5.1, 4.1) (6.7, 2.7), (8.0, 4.7).	25
Scenario 2	TAPF	Ditto	Ditto	(6.9, 8.2).	Infinite
	IAPF	Ditto	Ditto	(1.8, 6.7), (4.6, 7.6) (6.7, 8.4), (7.1, 8.2) (6.9, 8.2).	20

C. PATH UNSMOOTHNESS RESOLUTION
The path generated by the APF method has a great dependence on environmental factors such as obstacles and

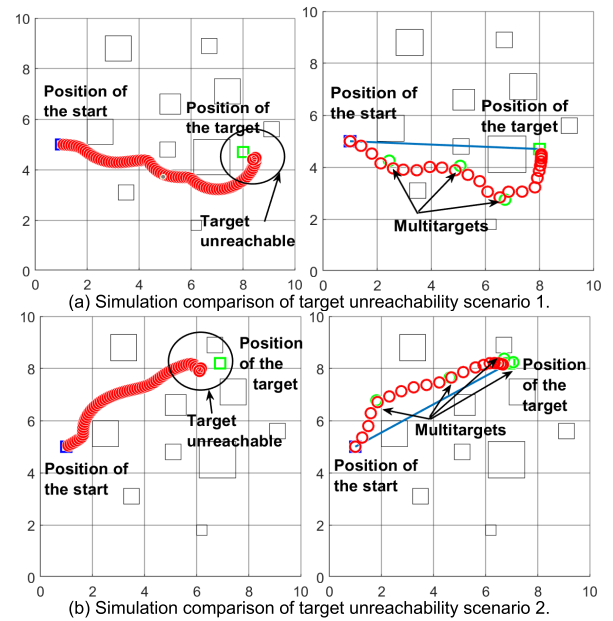targets, and the problem of turns with unsuitable large angle at some points may occur, and the path is not suitable for AMR for trajectory tracking, so smoothing of the path is necessary. In this paper, based on the safe driving corridor constructed on the planned path, the quadratic programming approach is used to generate a path that is completely constrained to the safe driving area. As shown in Fig. 12, in the scenarios of IV, the generated optimized trajectory does not collide with any obstacle, and becomes smoother.
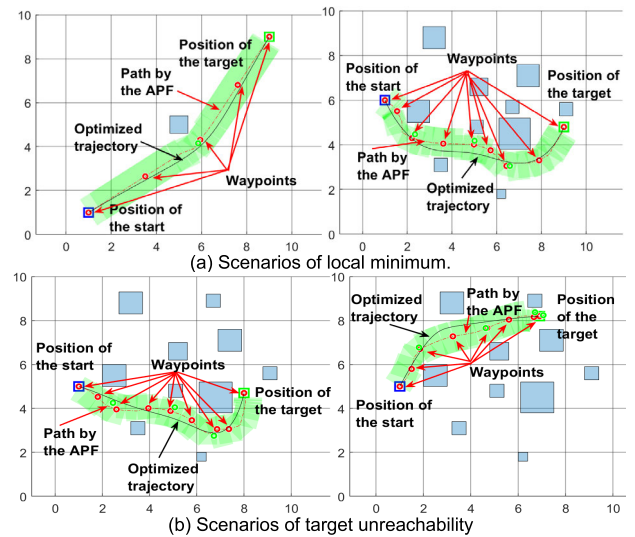

FIGURE 12. Optimized trajectory.

D. ANALYSIS OF SIMULATION RESULTS
Compared to the stagnant situation in traditional APF algorithm, the proposed improved APF algorithm

TABLE 4. Comparison of simulation results for DWA, TAPF and IAPF.

		Simulation 1	Simulation 2	Simulation 3	Simulation 4
DWA	Time of path planning(s)	0.629416	0.793274	0.729834	0.656724
	Smoothness	0.0173	0.037	0.0326	0.0399
	Iteration	51	91	71	69
TAPF	Time of path planning(s)	\	\	0.095480	0.119320
	Smoothness	\	1.2722	0.6761	0.4551
	Iteration	28	30	25	20
IAPF	Time of path planning(s) (compared with TAPF)	0.003293	0.009227	0.010177 (reduced by 89.34%)	0.006128 (reduced by 94.86%)
	Time of trajectory optimizing(s)	0.317348	0.465301	0.420400	0.321194
	Total time(s) (compared with DWA)	0.320641 (reduced by 49.06%)	0.474528 (reduced by 40.18%)	0.430577 (reduced by 41.00%)	0.327322 (reduced by 50.16%)
	Smoothness (compared with DWA)	0.0082 (increased by 52.60%)	0.0258 (increased by 30.27%)	0.0238 (increased by 26.99%)	0.0116 (increased by 70.93%)
	(compared with TAPF)	\	(increased by 97.97%)	(increased by 96.48%)	(increased by 97.45%)

Note: The number of iterations and time for TAPF path planning are the data when the AMR is stopped by falling into a local minimum or target unattainability situation. $smoothness = \sqrt{(\sum_{i=1}^{N-1}(\theta_{i+1} - \theta_i)^2)/(N-2)}$.

successfully avoids the problem of local minimum and reaches the target. In particular, when simulating in the multi-obstacle environment, the proposed improved APF analyzes the known environment information, selects the area with less collision risk, and uses the multi-target model to guide the AMR to reach the final target. The simulation experimental data of the above four scenarios are shown in Table 4, which contains the comparison experiments of IAPF with traditional APF and DWA path planning algorithms, where the evaluation indicator for smoothness is introduced. Compared with the traditional APF algorithm, the improved algorithm has fewer iterations. Except for the simulation of avoiding local minimum in the single obstacle situation, in the remaining scenarios the number of iterations of the improved algorithm is much less than half of the number of iterations of the traditional APF. Compared to recently published papers [14], [17], [25], [26], the proposed IAPF simultaneously overcomes several drawbacks of traditional APFs - falling into local minima, the goal unreachability problem, and path non-smoothing. The good results obtained from the experiments are a strong proof of the simplicity and effectiveness of the method in this work.

The improved algorithm has good real-time performance with path planning time within a few hundredths of a second, path optimization and trajectory generation time in the order of a fraction of a second on a moderately fast 7th generation i5 CPU computer.

V. CONCLUSION AND FUTURE WORK
In this paper, the author proposes an improved APF algorithm that not only considers the effect of obstacle size and shape on path smoothing and collision avoidance, but also adaptively adjusts the step size according to the distance and angle relationship with the obstacle within a certain range, and finally constructs safe driving corridors based on the generated path, so as to generate a smooth and collision-free path.

From the simulation results, it can be seen that the path smoothness of IAPF is improved by an average of 97.3% as compared to traditional APF and 45.19% as compared to DWA. The sum of the proposed IAPF path planning and optimization time is improved by 45.1% on average compared to DWA path planning time. The results show that the proposed improved algorithm is far superior to the traditional APF algorithm and DWA. Therefore, this algorithm can be used in cargo handling and mine transportation indoor or outdoor in unmanned factories, patrolling and even certain rescue situations. The path generated based on the multi-target model and quadratic planning is not only suitable for the AMR tracking, but also can reduce the distance and increase the speed to a certain extent in many complex scenarios.

There are still some shortcomings in the study. The adaptive step-size adjustment strategy based on the relationship between distance and angle to obstacles within the prediction range does not work well in some complex scenarios. At some point, it may occur sudden changes in the path due to improper step size adjustment. When constructing the multi-target, the selection of lateral safety distance only considers the obstacle size, and the obstacle type, motion state and other factors will be taken into consideration in the future research. In addition, the study in this paper only considers the static obstacle case. The combination of some intelligent algorithms in dynamic obstacle environments will be considered in the future research.

REFERENCES
[1] O. Khatib, "Real-time obstacle avoidance for manipulators and mobile robots," in *Proc. IEEE Int. Conf. Robot. Autom.*, Mar. 1985, pp. 500–505.

[2] C. W. Warren, "Global path planning using artificial potential fields," in *Proc. Int. Conf. Robot. Autom.*, May 1989, pp. 316–321.

[3] M. Cheol Lee and M. Gyu Park, "Artificial potential field based path planning for mobile robots using a virtual obstacle concept," in *Proc. IEEE/ASME Int. Conf. Adv. Intell. Mechatronics (AIM)*, Jul. 2003, pp. 735–740.

[4] J. Ji, A. Khajepour, W. W. Melek, and Y. Huang, "Path planning and tracking for vehicle collision avoidance based on model predictive control with multiconstraints," *IEEE Trans. Veh. Technol.*, vol. 66, no. 2, pp. 952–964, Feb. 2017.

[5] Y. Rasekhipour, A. Khajepour, S.-K. Chen, and B. Litkouhi, "A potential field-based model predictive path-planning controller for autonomous road vehicles," *IEEE Trans. Intell. Transp. Syst.*, vol. 18, no. 5, pp. 1255–1267, May 2017.

[6] B. Krogh and C. Thorpe, "Integrated path planning and dynamic steering control for autonomous vehicles," in *Proc. IEEE Int. Conf. Robot. Autom.*, Apr. 1986, pp. 1664–1669.

[7] Y. Koren and J. Borenstein, "Potential field methods and their inherent limitations for mobile robot navigation," in *Proc. IEEE Int. Conf. Robot. Autom.*, Apr. 1991, pp. 1398–1404.

[8] O. Cetin, I. Zagli, and G. Yilmaz, "Establishing obstacle and collision free communication relay for UAVs with artificial potential fields," *J. Intell. Robot. Syst.*, vol. 69, no. 1, pp. 361–372, Jan. 2013.

[9] Y.-B. Chen, G.-C. Luo, Y.-S. Mei, J.-Q. Yu, and X.-L. Su, "UAV path planning using artificial potential field method updated by optimal control theory," *Int. J. Syst. Sci.*, vol. 47, no. 6, pp. 1407–1420, Apr. 2016.

[10] U. Orozco-Rosas, O. Montiel, and R. Sepúlveda, "Pseudo-bacterial potential field based path planner for autonomous mobile robot navigation," *Int. J. Adv. Robot. Syst.*, vol. 12, no. 7, p. 81, Jul. 2015.

[11] S. S. Ge and Y. J. Cui, "New potential functions for mobile robot path planning," *IEEE Trans. Robot. Autom.*, vol. 16, no. 5, pp. 615–620, Oct. 2000.

[12] A. Sepehri and A. M. Moghaddam, "A motion planning algorithm for redundant manipulators using rapidly exploring randomized trees and artificial potential fields," *IEEE Access*, vol. 9, pp. 26059–26070, 2021.

[13] R. M. J. A. Souza, G. V. Lima, A. S. Morais, L. C. Oliveira-Lopes, D. C. Ramos, and F. L. Tofoli, "Modified artificial potential field for the path planning of aircraft swarms in three-dimensional environments," *Sensors*, vol. 22, no. 4, p. 1558, Feb. 2022.

[14] H. Li, "Robotic path planning strategy based on improved artificial potential field," presented at the *Proc. Int. Conf. Artif. Intell. Comput. Eng. (ICAICE)*, Oct. 2020, pp. 67–71.

[15] M. Shang, M. Chu, and M. Grethler, "Path planning based on artificial potential field and fuzzy control," in *Proc. Int. Conf. Intell. Comput., Autom. Syst. (ICICAS)*, Dec. 2020, pp. 304–308.

[16] Y. Ji, L. Ni, C. Zhao, C. Lei, Y. Du, and W. Wang, "TriPField: A 3D potential field model and its applications to local path planning of autonomous vehicles," *IEEE Trans. Intell. Transp. Syst.*, vol. 24, no. 3, pp. 3541–3554, Mar. 2023.

[17] R. Szczepanski, "Safe artificial potential field—Novel local path planning algorithm maintaining safe distance from obstacles," *IEEE Robot. Autom. Lett.*, vol. 8, no. 8, pp. 4823–4830, Aug. 2023.

[18] H. Li, W. Liu, C. Yang, W. Wang, T. Qie, and C. Xiang, "An optimization-based path planning approach for autonomous vehicles using the DynEFWA-artificial potential field," *IEEE Trans. Intell. Vehicles*, vol. 7, no. 2, pp. 263–272, Jun. 2022.

[19] Y. Shin and E. Kim, "Hybrid path planning using positioning risk and artificial potential fields," *Aerosp. Sci. Technol.*, vol. 112, May 2021, Art. no. 106640.

[20] J. Sfeir, M. Saad, and H. Saliah-Hassane, "An improved artificial potential field approach to real-time mobile robot path planning in an unknown environment," in *Proc. IEEE Int. Symp. Robot. Sensors Environ. (ROSE)*, Sep. 2011, pp. 208–213.

[21] Y. Zheng, X. Shao, Z. Chen, and J. Zhang, "Improvements on the virtual obstacle method," *Int. J. Adv. Robot. Syst.*, vol. 17, no. 2, Mar. 2020, Art. no. 1729881420911763, doi: 10.1177/1729881420911763.

[22] F. Matoui, B. Boussaid, and M. N. Abdelkrim, "Distributed path planning of a multi-robot system based on the neighborhood artificial potential field approach," *Simulation*, vol. 95, no. 7, pp. 637–657, Jul. 2019.

[23] Y. Duan, C. Yang, J. Zhu, Y. Meng, and X. Liu, "Active obstacle avoidance method of autonomous vehicle based on improved artificial potential field," *Int. J. Adv. Robot. Syst.*, vol. 19, no. 4, Jul. 2022, Art. no. 1729880622115984, doi: 10.1177/17298806221115984.

[24] R. Szczepanski, A. Bereit, and T. Tarczewski, "Efficient local path planning algorithm using artificial potential field supported by augmented reality," *Energies*, vol. 14, no. 20, Oct. 2021, Art. no. 20.

[25] Q. Yao, Z. Zheng, L. Qi, H. Yuan, X. Guo, M. Zhao, Z. Liu, and T. Yang, "Path planning method with improved artificial potential field—A reinforcement learning perspective," *IEEE Access*, vol. 8, pp. 135513–135523, 2020.

[26] R. Szczepanski, T. Tarczewski, and K. Erwinski, "Energy efficient local path planning algorithm based on predictive artificial potential field," *IEEE Access*, vol. 10, pp. 39729–39742, 2022.

[27] A. Azzabi and K. Nouri, "An advanced potential field method proposed for mobile robot path planning," *Trans. Inst. Meas. Control*, vol. 41, no. 11, pp. 3132–3144, Jul. 2019.

[28] T. Guo, J. Wang, Z. Wang, W. Chen, G. Chen, and S. Zhang, "Research on path planning of mobile robot with a novel improved artificial potential field algorithm," *Math. Problems Eng.*, vol. 2022, pp. 1–13, Sep. 2022.

[29] Y. Li, W. Yang, X. Zhang, X. Kang, and M. Li, "Research on automatic driving trajectory planning and tracking control based on improvement of the artificial potential field method," *Sustainability*, vol. 14, no. 19, Sep. 2022, Art. no. 19.

[30] L. Zhai, X. Zhang, X. Zhang, and C. Wang, "Local dynamic obstacle avoidance path planning algorithm for unmanned vehicles based on potential field method," *Trans. Beijing Inst. Technol.*, vol. 42, no. 7, pp. 696–705, 2022.

[31] J. Song, C. Hao, and J. Su, "Path planning for unmanned surface vehicle based on predictive artificial potential field," *Int. J. Adv. Robot. Syst.*, vol. 17, no. 2, Mar. 2020, Art. no. 1729881420918461, doi: 10.1177/1729881420918461.

[32] J. Batista, D. Souza, J. Silva, K. Ramos, J. Costa, L. dos Reis, and A. Braga, "Trajectory planning using artificial potential fields with metaheuristics," *IEEE Latin Amer. Trans.*, vol. 18, no. 5, pp. 914–922, May 2020.

[33] H. Sang, Y. You, X. Sun, Y. Zhou, and F. Liu, "The hybrid path planning algorithm based on improved A* and artificial potential field for unmanned surface vehicle formations," *Ocean Eng.*, vol. 223, Mar. 2021, Art. no. 108709.

[34] S. A. A. Shahidian and H. Soltanizadeh, "Path planning for two unmanned aerial vehicles in passive localization of radio sources," *Aerosp. Sci. Technol.*, vol. 58, pp. 189–196, Nov. 2016.

[35] J. Chen, K. Su, and S. Shen, "Real-time safe trajectory generation for quadrotor flight in cluttered environments," in *Proc. IEEE Int. Conf. Robot. Biomimetics (ROBIO)*, Dec. 2015, pp. 1678–1685.

[36] J. Chen, T. Liu, and S. Shen, "Online generation of collision-free trajectories for quadrotor flight in unknown cluttered environments," in *Proc. IEEE Int. Conf. Robot. Autom. (ICRA)*, May 2016, pp. 1476–1483.

[37] F. Gao, W. Wu, Y. Lin, and S. Shen, "Online safe trajectory generation for quadrotors using fast marching method and Bernstein basis polynomial," in *Proc. IEEE Int. Conf. Robot. Autom. (ICRA)*, May 2018, pp. 344–351.

JIE YANG received the B.S. degree in vehicle engineering from Xihua University, Chengdu, China, in 2021. He is currently pursuing the M.S. degree in vehicle engineering with the Wuhan University of Technology, Wuhan, China. His research interests include path planning and trajectory optimization for AMR.

HONGCHANG ZHANG received the B.S. and M.S. degrees from the Wuhan University of Technology, in 2002 and 2006, respectively, and the Ph.D. degree from Huazhong University of Science and Technology, Wuhan, China, in 2012. Since 2015, he has been with the Wuhan University of Technology, where he is currently an Associate Professor with the School of Automotive Engineering. His research interests include research on automotive active safety technology, research and application of sensor detection (environment sensing) technology, research and application of connected vehicle technology, and design and development of automotive electronic control systems.

PENG NING received the B.S. degree in automobile service engineering from the Nanjing Institute of Technology, Nanjing, China, in 2021. He is currently pursuing the M.S. degree in vehicle engineering with the Wuhan University of Technology, Wuhan, China. His research interests include decision-making, trajectory planning, and control of autonomous vehicles.